View metadata, citation and similar papers at core.ac.uk
brought to you by CORE
provided by Repositorio Universidad de Zaragoza

Interfacing transition metal dichalcogenides with carbon nanodots for managing photoinduced energy and charge-transfer processes

Lorenzo Vallan,[‡#] Ruben Canton-Vitoria,[§#] Habtom B. Gobeze,[¶#] Youngwoo Jang,[¶] Raul Arenal,[*$, ¥] Ana M. Benito,[‡] Wolfgang K. Maser,[*‡] Francis D' Souza,[*¶] Nikos Tagmatarchis[*§]

[§] Theoretical and Physical Chemistry Institute, National Hellenic Research Foundation, 11635 Athens, Greece.

[‡] Instituto de Carboquímica, Consejo Superior de Investigaciones Científicas, 50018 Zaragoza, Spain.

[¶] Department of Chemistry, University of North Texas, 305070 Denton, TX 76203-5017, USA.

[$] Laboratorio di Microscopias Avanzadas, Instituto de Nanociencia de Aragon, Universidad de Zaragoza, 50018 Zaragoza, Spain.

[¥] ARAID Foundation, 50018, Zaragoza, Spain.

ABSTRACT: Exfoliated semiconducting MoS_2 and WS_2 were covalently functionalized with 1,2-dithiolane-modified carbon nanodots (CNDs). The newly synthesized CND-MoS_2 and CND-WS_2 hybrids were characterized by spectroscopic, thermal and electron microscopy imaging methods. Based on electronic absorption and fluorescence emission spectroscopy, modulation of the optoelectronic properties of TMDs by interfacing with CNDs was accomplished. Electrochemical studies revealed facile oxidation of MoS_2 over WS_2 in the examined hybrids, suggesting it to be better electron donor. Excited state events, investigated by femtosecond transient absorption spectroscopic studies, revealed ultrafast energy transfer from photoexcited CNDs to both MoS_2 and WS_2. Interestingly, upon MoS_2 photoexcitation charge transfer from an exciton dissociation path of MoS_2 to CNDs, within CND-MoS_2, was observed. However, such process in CND-WS_2 was found to be absent due to energetic reasons. The present study highlights the importance of TMD-derived donor-acceptor hybrids in light energy harvesting and optoelectronic applications. Furthermore, the fundamental information obtained from the current results will benefit design strategies and impact the development of additional TMD-based hybrid materials to efficiently manage and perform in electron-transfer processes.

INTRODUCTION

Carbon nanodots (CNDs) are recognized as promising materials for energy conversion applications.[1-3] In general, CNDs are photochemically stable,[4] show varied solubilty in aqueous and organic media[5] and possess size in the order of 1-10 nm.[6, 7] The CNDs are abundantly prepared by economic, facile and environmental benign routes, mainly involving polycondensation reactions of small organic molecules at medium or elevated temperatures under hydrothermal or microwave irradiation conditions.[8-10] Importantly, the surface of CNDs can be decorated with diverse functional units, which can serve as anchors to conjugate other species en route the preparation of functional hybrid nanomaterials. Notably, depending on the precursors employed for the synthesis, the periphery of the surface of CNDs can be decorated with diverse functional units, which can serve as anchors to conjugate other species en route the preparation of functional hybrid nanomaterials. For example, CNDs have been covalently conjugated with carbon nanotubes,[11] porphyrins[12] and extended tetrathiafulvalene (exTTF)[13] and found to participate in photoinduced charge-transfer processes. Among the marked characteristics of CNDs are the broad and tunable absorption in the visible region and the intrinsic photoluminescence,[14] while interestingly, CNDs can act as either electron donors or acceptors, owed to their bivalent redox character.[15] This is to say that upon photoirradiation, CNDs donate electrons when assembled with carbon nanotubes or perylenediimides,[11, 16, 17] and accept electrons upon interaction with porphyrins and exTTF.[12, 13, 18]

Conversely, the fascination of transition metal dichalcogenides (TMDs) for energy-related applications,[19-22] attributed to their astounding optoelectronic properties and high electrical conductivity[23] has become progressively apparent. Molybdenum disulfide MoS_2 and tungsten disulfide WS_2, as the most fascinated and examined TMDs, consist of an atomic thick layer of transition metals sandwiched by two atomic layers of sulfur atoms.[24, 25] Even though the crystal structure of TMDs can greatly vary, depending on the number of d-electrons of the transition metal, the most commonly observed polytypes are those with trigonal prismatic D_{3h} symmetry possessing semiconducting properties and with octahedral O_h coordination which show metallic behavior.[26] Delaminated TMDs can be obtained by exfoliation of the bulk counterpart and depending on the exfoliating agent employed, different polytypes are derived. For instance, treatment of bulk TMDs with organometallic media results to the metastable metallic polytype which converts to the semiconducting one by annealing, with electron-transfer phenomena governing the exfoliation process.[27-31] On the other hand, chlorosulfonic acid acting as Bronstead acid partially protonates the sulfur atoms of MoS_2 and WS_2, without oxidizing them, yielding semiconducting exfoliated nanosheets due to the

development of repulsive electrostatic forces between the layers of TMDs.[32]

Managing and controlling the electronic properties of semiconducting TMDs, which are governed by excitonic transitions, is mandatory for their realization as prototype devices in energy-related applciations. To this end, among other sophisticated and complicated processes employed in nanosized semiconducting materials, a facile yet straightforward approach to gain precise control over the optoelectronic properties is by decorating the surface of TMDs with photo- and/or electro-active species and tuning the charge-carrier density.[33] Hence, covalent functionalization unlocks the potentiality of TMDs by opening new opportunities and broadening the spectrum of applications.[34-39] In a prominent example, exploiting the high binding affinity of 1,2-dithiolanes for transition metal atoms with chalcogen vacant sites, the covalent functionalization of exfoliated semiconducting TMDs was accomplished.[39] Nevertheless, interfacing TMDs with photoactive species via robust covalent bonding toward the development of advanced hybrid materials has yet to be fully advanced. Veritably, the development of such hybrids is timely and surely deserves investigation, especially in the context of their ability to function as donor-acceptor systems upon photoillumination.

With all the above in mind, CNDs and TMDs as two highly promising nanomaterials for energy conversion, each one possessing unique characteristics and properties, were combined via robust covalent bonding en route the realization of novel donor-acceptor hybrids. Specifically, herein we report on the conjugation of modified CNDs incorporating 1,2-dithiolane moieties at the edges of exfoliated semiconducting MoS_2 and WS_2 and perform a comprehensive photophysical study. With the current approach, modulation and engineering of the optoelectronic properties of photoexcited TMDs was accomplished, by employing CNDs as electron acceptors, via photoinduced electron transfer processes to occur from MoS_2, but not from WS_2 to CNDs. The newly prepared CND-MoS_2 and CND-WS_2 hybrid materials were fully characterized by complementary spectroscopic, thermal and electron microscopy imaging means, undoubtfully verifying the structures derived by the functionalization process. The optical and redox properties of CND-MoS_2 and CND-WS_2 were probed by electronic absorption, fluorescence emission spectroscopy and electrochemistry, respectively, revealing the existence of excited state intrahybrid electronic interactions between the two species, while also showing that MoS_2 was a better electron donor compared to WS_2. Furthermore, with the aid of femtosecond transient spectroscopy by exciting the TMD part within the hybrid materials, strong electronic interactions between the two species leading to photoinduced charge-separation only within CND-MoS_2 but not for CND-WS_2 were identified. In addition, upon excitation of CNDs in CND-TMD ultrafast energy transfer from excited CNDs to both MoS_2 and WS_2 was identified. The fundamental information obtained from the current study will impact the development of additional TMD-based hybrid materials to efficiently manage and perform in electron-transfer processes aiming to photovoltaic and solar energy related applications.

RESULTS AND DISCUSSION

Initially, CNDs featuring plethora of free amine groups were prepared by polycondensation of citric acid and ethylenediamine, followed by addition of butylamine. The latter enhances the lipophilicity of CNDs, by introducing butyl units, while at the same time consumes all remaining carboxylic acid groups, stopping the growth of the nanoparticles. Next, lipoic acid activated by (3-dimethylaminopropyl)-N′-ethylcarbodiimide was condensed to yield modified CNDs bearing 1,2-dithiolanes as substituents on the periphery of their structure. Spectroscopic characterization by ^{1}H NMR and IR (Supporting Information, Figures S1, S2) verified the structure of modified CNDs and the success of synthesis. Further proof was delivered by the Kaiser test, where the amount of free amines on CNDs decreased significantly upon condensation with lipoic acid, from 1810 to 72 μmol/g. In parallel, bulk MoS_2 and WS_2 were wet exfoliated by chlorosulfonic acid,[32] and following the functionalization methodology for TMDs with 1,2-dithiolanes,[39-41] the conjugation of modified CNDs was accomplished, furnishing CND-MoS_2 and CND-WS_2 according to Scheme 1.

Scheme 1. Illustrative preparation of CND-MoS_2 and CND-WS_2 upon covalent 1,2-dithiolane functionalization of exfoliated semiconducting MoS_2 and WS_2 nanosheets.

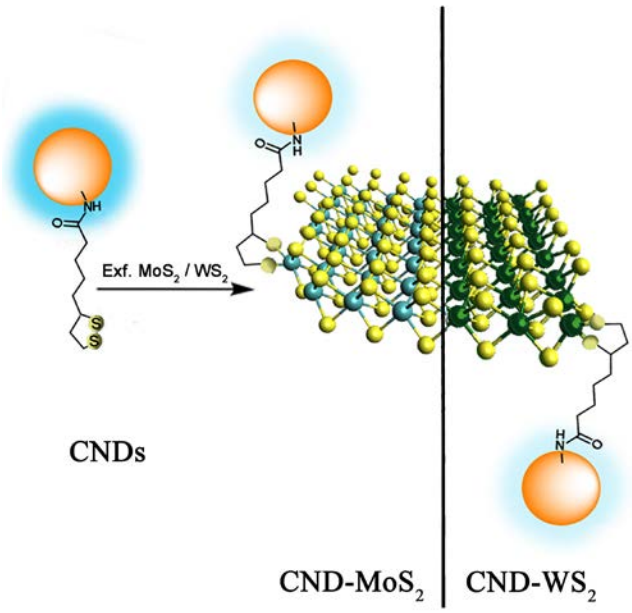

The newly derived hybrid materials found to be soluble in xxx (xxx mg/mL), xxx (xxx mg/mL) and xxx (xxx mg/mL), while remained insoluble in xxx and xxx. Notably, the solubility of both CND-MoS_2 and CND-WS_2 in xxx remained unchanged for a period of several months, evidenced by the absence of any precipitation, hence proving their high stability.

Next, complementary characterization of CND-MoS_2 and CND-WS_2 by IR and Raman spectroscopy, thermogravimetric analysis (TGA) and transmission electron microscopy (TEM) imaging was performed. The presence of characteristic bands at 1640 and 1550 cm^{-1}, related with stretching and bending modes of carbonyl amide vibrations, were evident in the ATR-IR spectrum of CND-MoS_2 and CND-WS_2 (Supporting Information, Figure S3). In addition, C-H stretching vibrations at 2960 and 2915 cm^{-1} due to the alkyl chain of 1,2-dithiolane were present.

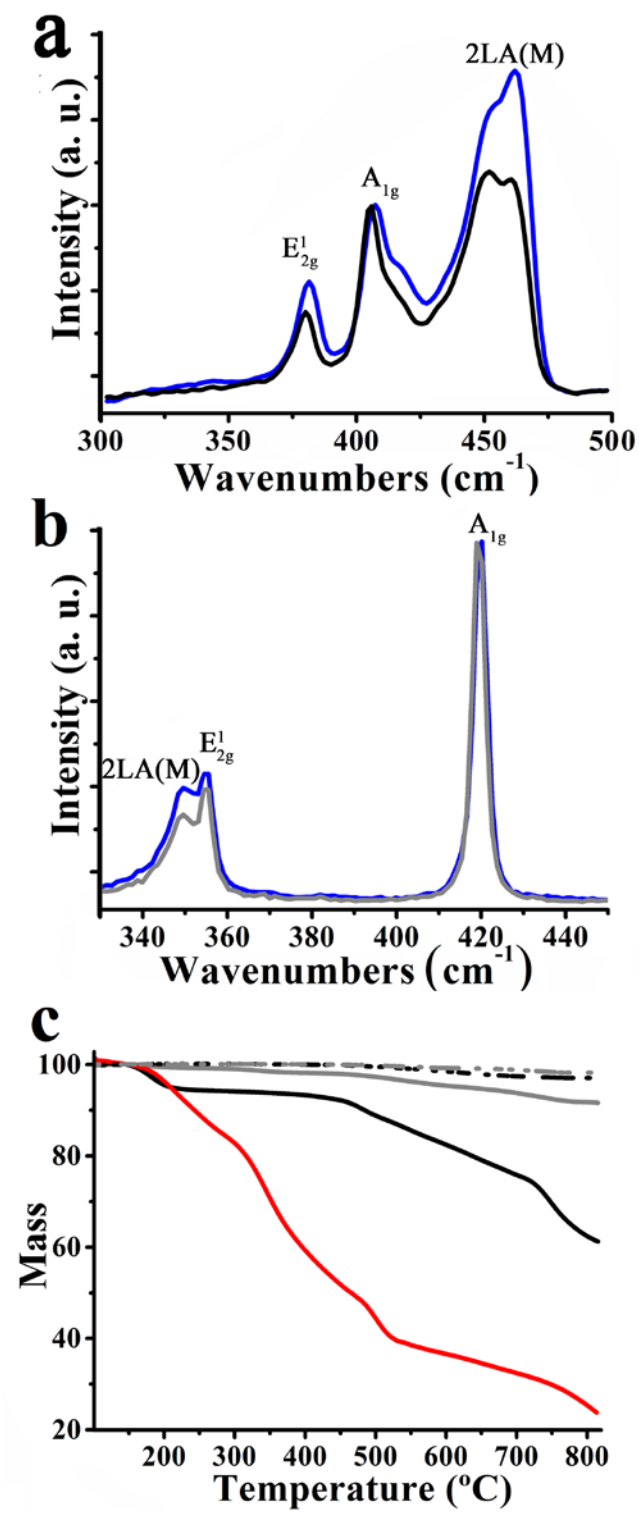

Figure 1. Raman spectra normalized at A^1_g mode for (a) exfoliated MoS_2 (blue) and CND-MoS_2 (black) at λ_{exc} 633 nm, and (b) exfoliated WS_2 (blue) and CND-WS_2 (grey) at λ_{exc} 514 nm. (c) Thermographs for CNDs (red), exfoliated MoS_2 (dotted black), exfoliated WS_2 (dotted gray), CND-MoS_2 (black), and CND-WS_2 (grey).

Comparing Raman spectra of exfoliated MoS_2 and CND-MoS_2, obtained upon excitation under on-resonance conditions at 633 nm and normalized at the A_{1g} mode at 404 cm^{-1}, it was found that the intensity of the 2LA(M) band associated to disorder and defects[42] and located at 447 cm^{-1} was found decreased in CND-MoS_2 as compared to that owed to exfoliated MoS_2 (Figure 1a).[36, 43] The latter comes as a result of the reduced number of S defects due to edge functionalization of MoS_2.[39] Moreover, the absence of the characteristic phonon modes of metallic polytype MoS_2 so-called J_1, J_2 and J_3 at 150, 225 and 325 cm^{-1}, respectively,[44, 45] ascertained the semiconducting behavior of MoS_2 in the CND-MoS_2 hybrid material. Regarding CND-WS_2, bands due to 2LA(M), E^1_{2g}, and A_{1g}, upon on-resonance excitation at 514 nm, were evident at 350, 354 and 419 cm^{-1}, with the intensity of the 2LA(M) mode decreased by 20% as compared to exfoliated WS_2 (Figure 1b). Furthermore, for both CND-MoS_2 and CND-WS_2, the A_{1g} and E^1_{2g} modes found red-shifted by 1-2 cm^{-1} as compared to the values registered for exfoliated MoS_2 and WS_2 respectively. The latter is attributed to intrahybrid charge-transfer phenomena developed between the CNDs and the TMDs, in accordance with literature reports.[46, 47] Since CNDs are highly fluorescent, weak and broad Raman bands attributed to –NC=O, C=O and C-H units were observed for both CND-MoS_2 and CND-WS_2 only upon excitation at 1064 nm (Supporting Information, Figure S4).

The loading of CNDs conjugated onto MoS_2 and WS_2 in CND-MoS_2 and CND-WS_2 was evaluated by TGA (Figure 1c). The modified CNDs bearing 1,2-dithiolane units were thermally stable up to 200 ºC under nitrogen atmosphere, while they lost 65% of mass at the temperature range 200-500 ºC. Since MoS_2 and WS_2 are thermally stable in that temperature range, the observed mass loss for CND-MoS_2 and CND-WS_2, 7.5% and 3.0% respectively, is related to the decomposition of modified CNDs present in the two hybrids. Although this is a relatively small mass loss, it is consistent with the edge functionalization of the limited S vacant sites of MoS_2 and WS_2.[39]

The CND-MoS_2 and CND-WS_2 hybrids were morphologically imaged by HR-TEM. A few drops of a dispersion of the materials in hexane were deposited on the TEM grid and imaged after the solvent was evaporated. Extensive imaging of several different areas and flakes of the CND-MoS_2 and CND-WS_2 hybrid materials revealed that the size of MoS_2 and WS_2 is in the order of few hundred nanometres, e.g. around 200-400 nm (Supporting Information, Figure S4). Although mostly oligolayered flakes were observed, most likely due to restacking of the TMDs during the drying process of the sample after depositing it on the TEM grid, the presence of some monolayered ones were also identified. In order to get better insight on CND-MoS_2 and CND-WS_2, TEM studies complemented with spatially-resolved electron energy loss spectroscopy (EELS) were performed. Figures 2a and 2f show high angle annular dark field (HAADF) scanning TEM (STEM) micrographs for CND-MoS_2 and CND-WS_2, respectively. Based on the following spectroscopic/chemical TEM analyses, the bright small objects observed in these images was assigned to CNDs covalently anchored on TMD flakes. This is confirmed by energy dispersive X-ray spectroscopy (EDS) analyses (Figures 2b, g) and EELS (Figures 2c-e and 2h-j). Figure 2c displays an ADF micrograph of CND-MoS_2 and an EELS spectrum-image (SPIM) was recorded in the red marked rectangular area. Three EEL spectra were extracted in the highlighted square regions (Figure 2e(i)-(iii)). Each of these three EEL spectra corresponds to the sum of 9 spectra (3x3 probe positions of the SPIM). The S-$L_{2,3}$ and Mo-M edges are visible in the three spectra and correspond to MoS_2.[48, 49] It is worth mentioning that no MoO_x was observed highlighting the

high quality and purity of the materials. In addition, C was detected in specific areas, see the presence of the C-K edge (Figure 2e(ii)-(iii)). This C-K edge, which is superposed to the Mo-$M_{4,5}$ edge, is associated with the presence of CNDs within the CND-MoS_2 hybrid. The chemical C map obtained from the analysis of C-K edge (Figure 2d) clearly supports this finding.[48, 49] Indeed, CNDs are observed not only in the ADF-STEM micrograph (Figure 2c) but also in this C-map (Figure 2d). Similar assays were performed for CND-WS_2 and from TEM analyses (Figures XXX Sup. Inf) the presence of CNDs attached on WS_2 was confirmed.

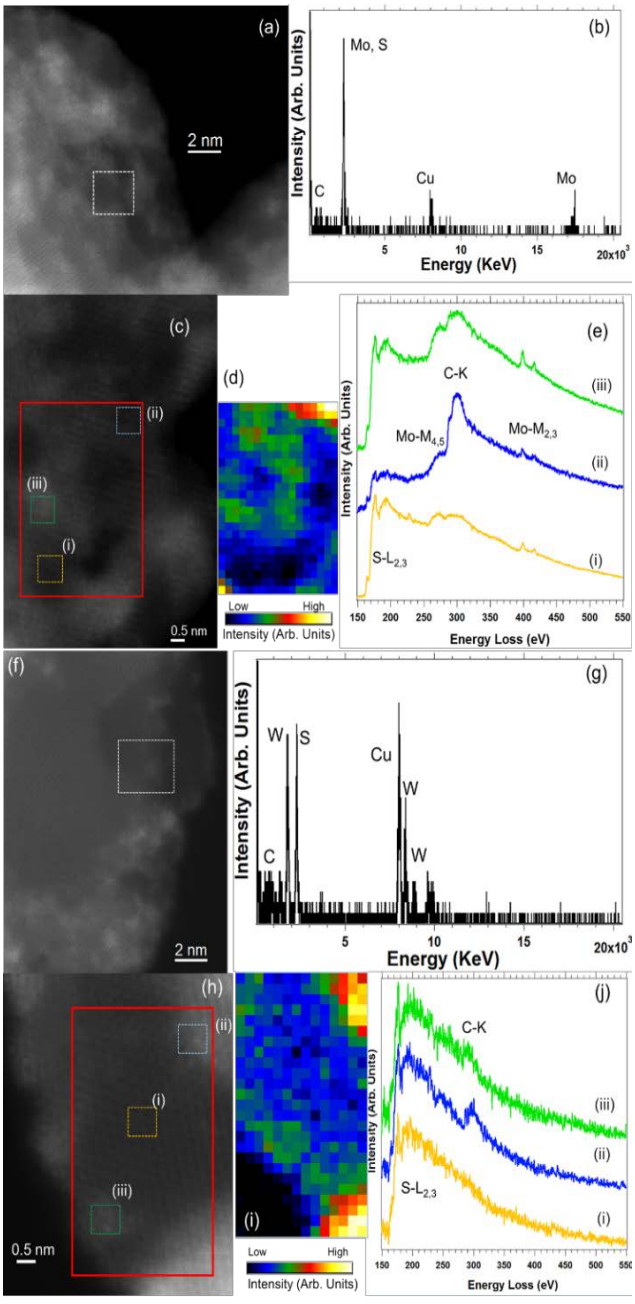

Figure 2. Representative HRSTEM-ADF images for (a, d) CND-MoS_2, and (f, h) CND-WS_2. (b, g) EDS on the squared white areas in (a, f), respectively. In the red regions of (c, h) spectrum-images SR-EELS were recorded. (d, i) Carbon elemental mapsextracted from the integrated intensity of the C-K edge of the two EELS spectra-image recorded in the red areas in (c, h). (e) Three spectra from the sum of 9 (3x3) EELS extracted from the marked areas of the EELS SPIM of (c). The C-K edge (~284 eV) is obs erved in (ii) and (iii) superposed with the Mo-M edge. The S-$L_{2,3}$ and Mo-M edge of MoS_2 are visible in the 3 spectra ((i)-(iii)). (j) Similar analysis for CND-WS_2 as in (e). Three spectra from the sum of 16 (4x4) EELS extracted from the EELS SPIM of (h), showing the S-$L_{2,3}$ and C-K (in this case only in (ii) and (iii)) edges.

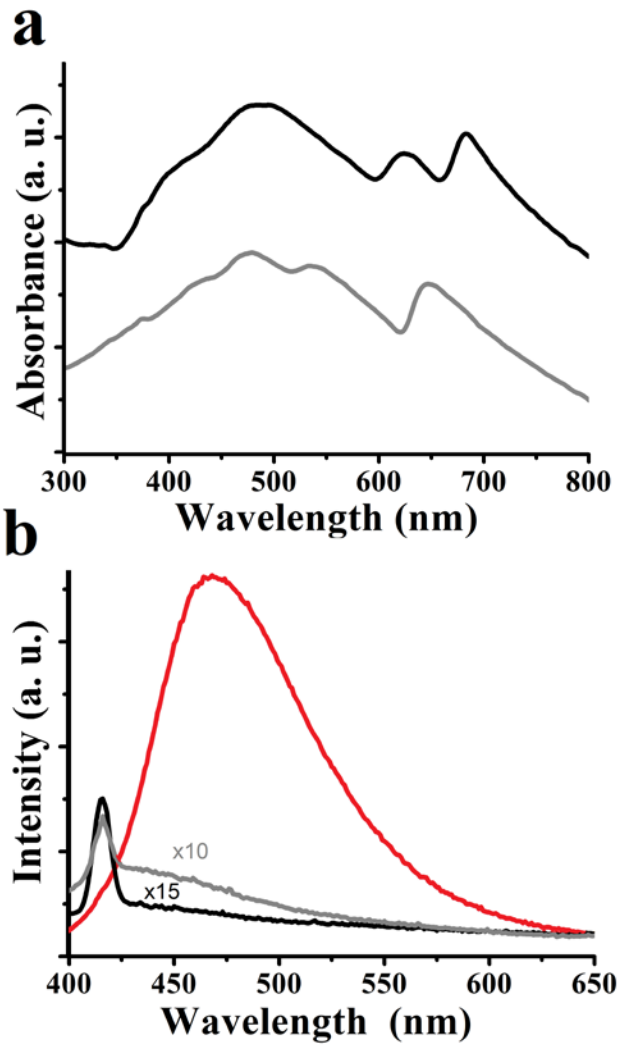

Figure 3. (a) Absorption and (b) emission spectra (λ_{exc} 370 nm) of CND-MoS_2 (black), CND-WS_2 (grey) and modified CNDs (red), in DMF.

Focusing on the optical properties of CND-MoS_2 and CND-WS_2, electronic absorption and fluorescence assays were conducted. In more detail, in the UV-Vis spectra of CND-MoS_2 and CND-WS_2 characteristic bands centered at 680, 620, 485, 400 nm, and 645, 535, 475, 420 nm, respectively, corresponding to semiconducting MoS_2 and WS_2, in addition to continuous absorption throughout the visible region due to the presence of both TMDs and CNDs, were seen (Figure 3a). Unfortunately, the strong absorption features of TMDs masked the broad band of modified CNDs, appearing at 370 nm (Supporting Information, Figure S5), hence hampering to defer conclusive statements regarding possible intrahybrid electronic

communication between the two species in the ground state. Nevertheless, the situation is rather clear in the excited state, where the strong emission of modified CNDs, centred at 470 nm upon excitation at 370 nm, was found blue-shifted by 30 nm, at 440 nm, and quantitatively quenched in both CND-MoS_2 and CND-WS_2 (Figure 3b). The later postulates the occurrence of an additional deactivation path for the singlet excited state of CNDs, through an energy or charge-transfer process. Next, analysis of the fluorescence emission decay profiles at 450 nm for the singlet excited state of CNDs upon excitation at 376 nm, gave a monoexponentially fitted lifetime of 6.3 ns. However, the corresponding analysis for CND-MoS_2 and CND-WS_2 resulted in a biexponential decay, with the identification of major faster components with 1.2 and 1.1 ns lifetime, corresponding to the quenching of singlet excited state of CNDs in CND-MoS_2 and CND-WS_2, respectively.

The electrochemical behavior of CND-MoS_2 and CND-WS_2 was successively investigated in DMF (Supporting Information, Figure S6). The cyclic voltammogram (CV) of exfoliated MoS_2 revealed irreversible oxidations at E_{pa} = -0.08 and 0.48 V and reductions at E_{pc} = -1.20 and -1.69 V vs Fc/Fc^+. In CND-MoS_2, the first oxidation wave was too broad to pick the peak potential, while the second one was better defined with an E_{pa} = 0.54 V. The two reductions were located at E_{pc} = -1.48 and -2.20 V as a consequence of the covalent functionalization. The CV of exfoliated WS_2 revealed irreversible oxidations at E_{pa} = 0.23 and 0.44 V and reductions at E_{pc} = -1.40 and -1.98 V. Upon covalent attachment of CNDs, the oxidation waves broadened, making it difficult to identify the peak potential, while the reduction was anodically shifted to E_{pc} = -1.37 and -1.63 V. Importantly, both MoS_2 and WS_2 were found to be electroactive and such property persisted upon chemical functionalization with CNDs. The facile oxidation of MoS_2 over WS_2 suggests it to be better electron donor. The CV of CNDs revealed no measurable electrochemical activity within the potential window. Differential spectral changes observed during the first oxidation and reduction of MoS_2 and WS_2 are shown at the Supporting Information, Figure S7. In both TMDs, reduction in peak intensity of the neutral species was observed, more so for MoS_2 compared to WS_2. Some positive spectral features in the 300-450 nm range were observed for MoS_2 during oxidation.

The excited state events were probed by femtosecond pump-probe transient absorption spectroscopy in DMF, where dispersion of the hybirds was appreciable. The samples were excited at 370 nm corresponding mainly to CNDs excitation and at 425 nm corresponding mainly to TMDs excitation. In agreement with literature reports,[50-52] immediately after 425 nm excitation of exfoliated MoS_2, three minima at 503, 637 and 696 nm due to excitonic transitions as seen in the absorption spectrum, and two maxima at 595 and 663 nm corresponding to induced absorption of B and A excitons, were observed (Supporting Information, Figure S8a). During the first 10 ps, all peaks experienced blue shift ascribed to cooling of hot excitons and/or interexcitonic interactions. In the case of exfoliated WS_2, two minima at 545, and 652 nm (B and A excitons, by comparison with the absorption spectrum) and two maxima at 516 and 617 nm were observed (Supporting Information, Figure S8b). The peak positions also experienced a small blue-shift of 2 nm within the first 10 ps.

Figure 4 shows the transient absorption spectra and intensity-wavelength maps of CND-MoS_2 and CND-WS_2 dispersions in DMF at λ_{exc} 370 nm mainly exciting the CNDs. The transient spectra of CNDs (λ_{exc} 370 nm) revealed positive peaks at 460 and 590 nm (Supporting Information, Figure S9a) originating from transitions involving excited CNDs. The decay of these peaks was rather slow consistent with the longer fluorescence lifetime of CNDs (6.3 ns). When exfoliated MoS_2 and WS_2 were excited at 370 nm (Supporting Information, Figure S9b, c), the spectra revealed features corresponding to these materials, however, with much diminished peak intensities compared to that shown in the Supoprting Information, Figure S9 at λ_{exc} 425 nm. These observations suggest that at λ_{exc} 370 nm, in addition to CNDs, both MoS_2 and WS_2 also get excited to some extent. Interestingly, when CND-MoS_2 and CND-WS_2 were excited at 370 nm, the peaks corresponding to the excited CNDs revealed rapid deactivation with simultaneous development of strong excitonic peaks of MoS_2 and WS_2, more so for CND-MoS_2 than that for CND-WS_2 (Figure 4). These results indicate occurrence of energy transfer from singlet excited CNDs to MoS_2 and WS_2 in the hybrids. In both hybrids the excitation transfer was complete within 4-5 ps, indicating an efficient process.

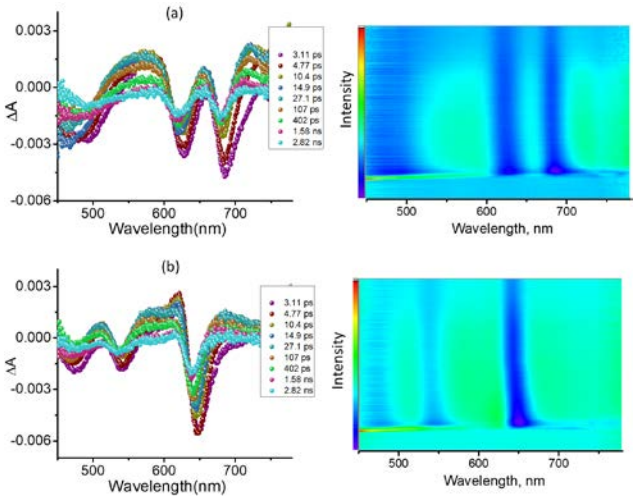

Figure 4. Femtosecond transient spectra of (a) CND-MoS_2, and (b) CND-WS_2 in DMF (λ_{exc} 370 nm). The right-hand panel shows intensity-wavelength maps.

Next, the hybrids were excited at 425 nm, where majority of MoS_2 and WS_2 have absorbance. The transient spectral features of CND-MoS_2 (Figure 5a) were distinctly different from that of exfoliated MoS_2 (Supporting Information, Figure S8a), especially with respect to the peak time profiles (see intensity-wavelength maps). Figure 5a(iii) shows the time profile of the 688 nm peak of exfoliated MoS_2 and CND-MoS_2 corresponding to the excitonic peak at 688 nm. The recovery of the exciton peak was slow for CND-MoS_2 suggesting occurrence of excited state events from the excited MoS_2 to the covalently linked CNDs. Earlier, a facile oxidation was observed for MoS_2 (E_{pa} = -0.08 V) suggesting that it could act as an electron donor generating charge separated state.[53-56] In such an event, charge transfer from a dissociated excitonic state would be promoted to CNDs conduction band, generating a charge separated state. The hole in MoS_2 layer would recover slowly due to a charge recombination process.

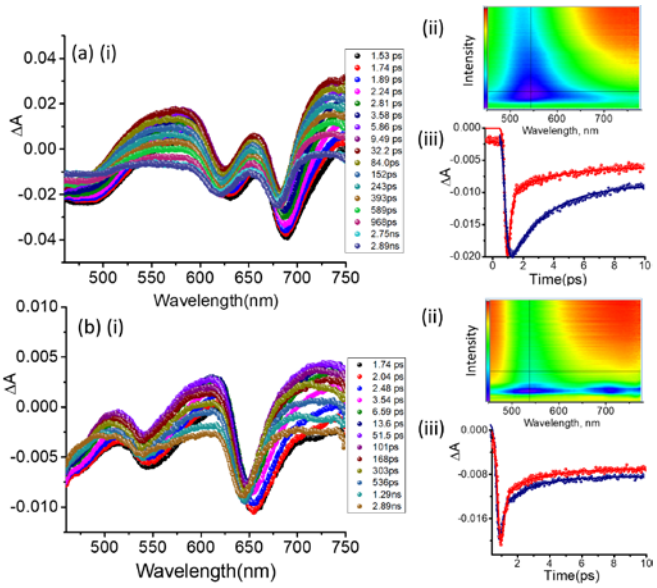

Figure 5. Femtosecond transient spectra of (a) CND-MoS_2, and (b) CND-WS_2, in DMF (λ_{exc} 425 nm). The right-hand panels show (ii) intensity-wavelength map and (iii) an overlap time profile of the 688 nm of CND-MoS_2 (blue) and exfoliated MoS_2 (red) and 652 nm of CND-WS_2 (blue) and exfoliated WS_2 (red).

Further, the transient data of exfoliated MoS_2 and CND-MoS_2 were subjected to global analysis for kinetic evaluations (Figure 6). Decay associated spectra of exfoliated MoS_2 revealed three major components; the spectrum at 2.3 ps consists of positive peaks at the spectral range, where excitonic peaks are expected. The spectrum at 1.1 ns had decay of positive transients. The final component with over 3 ns related to only the excitonic signals with positive shift relative to A exciton. Earlier, for the ultimate decay of the excitons, a lifetime of around 30 ns was established.[50] Interestingly, for CND-MoS_2, at least 5 components were needed for satisfactory fit. The component at 1 ps was too fast to be assigned to any excited state process as several ultrafast processes such as vibrational cooling, solvent relaxation, etc. occur. The 4.2 and 1.3 ps components had features of excitons in the growth and decay, respectively. The 246 ps component had features in the 450-550 nm range, ascribed to trionic state that revealed faster decay. The long-lived decay component had only the excitonic features similar to that observed for unmodified MoS_2. These results suggest that the charge separation occurs with a time constant of about 250 ps in the CND-MoS_2 hybrid.

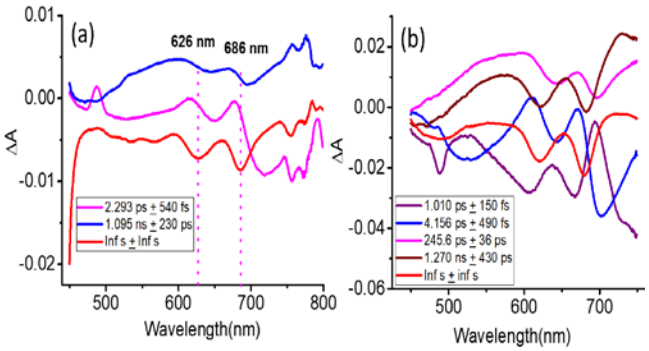

Figure 6. Decay associated spectra of (a) exfoliated MoS_2, and (b) CND-MoS_2 for the transient data shown in Figure S7a and Figure 5a.

Transient spectra recorded for CND-WS_2 (Figure 5b) were close to that of unmodified WS_2 (Supporting Information, Figure S8b). The time profiles of the 652 nm peak (Figure 5b(iii)) were superimposable suggesting lack of major excited state events such as charge transfer from excited WS_2 to CNDs. This could be rationalized to the harder oxidation of WS_2 (E_{pa} = 0.23) that would dampen any charge transfer events due to energy considerations. Hence, no further analysis was performed on this hybrid material.

CONCLUSIONS

In summary, following the 1,2-dithiolane functionalization protocol for TMDs, the covalent grafting of CNDs onto exfoliated MoS_2 and WS_2 was accomplished. The newly prepared CND-MoS_2 and CND-WS_2 hybrid materials were fully characterized by complementary spectroscopic, thermal and electron microscopy imaging techniques. Furthermore, electrochemical assays revealed that MoS_2 was a better electron donor compared to WS_2. Photochemical events upon preferential photoexcitation of CNDs and TMDs were probed. Excitation of CND-MoS_2 and CND-WS_2 at 370 nm revealed ultrafast energy transfer from excited CNDs to MoS_2 and WS_2, while exciting the TMDs within the hybrid materials at 425 nm, charge transfer in CND-MoS_2 but not in CND-WS_2 was seen. The observed excited state electron transfer processes bring us one-step closer to utilize the covalently modified TMDs in donor-acceptor type hybrids for energy harvesting applications.

EXPERIMENTAL SECTION

Electron microscopy imaging. STEM imaging and EELS studies were conducted using an aberration-corrected FEI Titan Low-Base microscope operated at 80 kV. This microscope was equipped with a Cs probe corrector and a Gatan Tridiem ESR 865 electron energy loss spectroscopy (EELS) spectrometer. The energy resolution was ~1 eV. The convergence and collection angles were 25 and 50 mrad, respectively. The EELS studies were conducted in STEM mode, using the spectrum-line scan mode. To increase the signal/noise ratio of the EEL spectra, the datasets were then de-noised with the open-source program Hyperspy by using principal component analysis routines.

Femtosecond transient absorption spectroscopy. Experiments were performed using an Ultrafast Femtosecond Laser Source (Libra series) by Coherent Inc. (Santa Clara, CA) incorporating diode-pumped, mode locked Ti:Sapphire laser (Vitesse) and diode-pumped intra cavity doubled Nd:YLF laser (Evolution) to generate a compressed laser output of 1.45 W. For optical detection, a Helios transient absorption spectrometer from Ultrafast Systems (Sarasota, FL) was used. The source for the pump and probe pulses were derived from the fundamental output of Libra (Compressed output 1.45 W, pulse width 100 fs) at a repetition rate of 1 kHz. About 95% of the fundamental output of the laser was introduced into a TOPAS-Prime-OPA system with 290-2600 nm tuning range from Altos Photonics Inc., (Bozeman, MT), while the rest of the output was used for generation of white light continuum. Kinetic traces at appropriate wavelengths were assembled from the time-resolved spectral data. Data analysis was performed using Surface Xplorer software supplied by Ultrafast Systems. All measurements were conducted in degassed solutions at room temperature.

Modified CNDs with lipoic acid. Initially, 2g of citric acid (1 equiv.) were dissolved in DMF (10 mL) and the solution was

cooled in ice bath. Then, 4.4 mL of *N,N'*-diisopropylcarbodiimide (DIC) as coupling agent (3 equiv.) were added slowly to the solution while stirring, forming a white dispersion. After one minute, 1.9 mL of ethylenediamine (EDA) in cold water (10 mL) were poured into the reaction mixture. When the color turned yellow and then orange the fluorescent particles were formed, thus butylamine (5 mL) was added and the reaction mixture was left under stirring for 24 hours. The addition of butylamine allowed the *in-situ* introduction of butyl groups on the CNDs surface, enhancing lipophilicity and at the same time consuming all remaining carboxylic groups, thus stopping the growth of the nanoparticles. Then, the solution was filtered to remove the DIC urea byproduct, the filtrate was washed three times with diethylether and the excess of butylamine was removed under vacuum evaporation. Finally, the water phase was purified by dialysis in ultrapure water (molecular weight cut-off = 0.5-1 kDa, 3 days). The dry product of CNDs-NH_2 (0.7 g) was obtained as a yellow powder by freeze-drying.

In the next step, CNDs-NH_2 (200 mg) were dissolved in a mixture of methanol (5 mL) and dichloromethane (25 mL) and cooled to 0 °C. In another flask, lipoic acid (300 mg) was dissolved in dichloromethane (5 mL), cooled at 0 °C and 336 mg of (3-dimethylaminopropyl)-N'-ethylcarbodiimide (EDC) were added. After 20 minutes, the lipoic acid solution was poured into that of CNDs-NH_2. The reaction mixture was left under stirring for 24 hours and after that period additional lipoic acid (100 mg) and EDC (56 mg) were added. After 3 hours the reaction mixture was extracted with distilled water, aqueous NaOH (pH=11) and with brine. The organic phase was dried over $MgSO_4$, the dichloromethane was partially evaporated by vacuum and diluted with ethyl acetate, resulting on the precipitation of the particles (centrifugation at 3200 rpm, 5 minutes). The redispersion-precipitation process was repeated until the lipoic acid spot in TLC disappeared. The precipitate was dissolved again in methanol/dichloromethane 1:1 v/v and dried over $MgSO_4$ to obtain CNDs carrying 1,2-dithiolane chains as a brown solid, after vacuum evaporation of the solvent.

Exfoliation of semiconducting TMDs. Bulk TMDs (150-200 mg) were dispersed in chlorosulfonic acid and sonicated for 2 hours at room temperature. The solution was left under stirring during a month, occasionally sonicated for 30 seconds. Afterwards it was added cold water to the solution under stirring, drop by drop and extremely carefully. Please notice that the reaction is exothermic and releases gaseous HCl. Next, the mixture was filtrated on a PTFE filter of 0.2 μm pore-size and washed with a good amount of methanol and acetone. The solid compound was added to N-methyl pyrrolidone and sonicated for 1 hour (tip sonication at 30-35% of amplitude (100% of 200 W)). After 3 days the supernatant was taken, filtrated on PTFE filter (0.2 μm pore-size) and washed with a large amount of methanol, acetone and dichloromethane.

CND-MoS_2 and CND-WS_2. The 1,2-dithiolane modified CNDs (50 mg) were dissolved in methanol (1 mL). In another flask, exfoliated TMDs (20 mg) were dispersed in DMF (10 mL) by sonication (10 min) and dropped in the CNDs solution. The flask was covered with aluminum foil and the reaction mixture was stirred at 70 °C for 4 days. After that period, it was cooled and filtered through a PTFE membrane (0.2 nm pore size). The solid residue was extensively washed with methanol and dichloromethane to obtain the CND-TMDs.

ASSOCIATED CONTENT

Supporting Information

General instrumentation, ^{1}H NMR, ATR-IR, Raman, UV-Vis and femtosecond transient absorption spectra and cyclic voltamograms. The Supporting Information is available free of charge on the ACS Publications website.

AUTHOR INFORMATION

Corresponding Author

* Email: tagmatar@eie.gr (N. Tagmatarchis)

* Email: Francis.DSouza@unt.edu (F. D'Souza)

* Email: wmaser@icb.csic.es (W. K. Maser)

* Email: arenal@unizar.es (R. Arenal)

Author Contributions

# These authors contributed equally.

ACKNOWLEDGMENT

This project has received funding from the European Union's Horizon 2020 research and innovation programme under the Marie Sklodowska-Curie grant agreement Nº 642742. Support of this work by the project "Advanced Materials and Devices" (MIS 5002409) which is implemented under the "Action for the Strategic Development on the Research and Technological Sector", funded by the Operational Programme "Competitiveness, Entrepreneurship and Innovation" co-financed by Greece (Ministry of Economy and Development, NSRF 2014-2020) and EU (European Regional Development Fund) to N. T. and the US-NSF (grant 1401188 to F. D.) is acknowledged. The HR-STEM and STEM-EELS studies were conducted at the Laboratorio de Microscopias Avanzadas, Universidad de Zaragoza, Spain. R. A. acknowledges support from Spanish MINECO grant MAT2016-79776-P (AEI/FEDER, UE) and from EU H2020 "Graphene Flagship" grant agreement 785219. W. K. M. and A. M. B. acknowledge Spanish MINECO grant ENE2016-79282-C5-1-R (AEI/FEDER, EU) and the Covernment of Aragon through project DGA-T03_17R (FEDER, EU).

ABBREVIATIONS

CNDs, carbon nanodots; exTTF, extended tetrathiafulvalene; TMDs, transition metal dichalcogenides; TGA, thermogravimetric analysis; TEM, transmission electron microscopy; EELS, electron energy loss spectroscopy; HAADF, high angle annular dark field; STEM, scanning transmission electron microscopy; EDS, energy dispersive X-ray spectroscopy.

REFERENCES

(1) Margraf, F. J.; Lodermeyer, T.; Strauss, V.; Haines, P.; Walter, J.; Peukert, W.; Costa, R. D.; Clark, T.; Guldi, D. M. Using carbon nanodots as inexpensive and environmentally friendly sensitizers in mesoscopic solar cells. *Nanoscale Horiz.* **2016**, *1*, 220-226.

(2) Martindale, B. C. M.; Joliat, E.; Bachmann, C.; Alberto, R.; Reisner, E. Clean donor oxidation enhances rhe H_2 evolution activity of a carbon quantum dot-molecular catalyst photosystem. *Angew. Chem. Int. Ed.* **2016**, *55*, 9402-9406.

(3) Li, X.; Rui, M.; Song, J.; Shen, Z.; Zeng, H. Carbon and graphene quantum dots for optoelectronic and energy devices: A review. *Adv. Funct. Mater.* **2015**, *25*, 4929-4947.

(4) Data, K. K. R.; Qi, G.; Zboril, R.; Giannelis, E. P. Yellow emitting carbon dots with superior colloidal, thermal, and photchemkical stabilities. *J. Mater. Chem. C* **2016**, *4*, 9798-9803.

(5) Gu, J.; Hu, D.; Huang, J.; Zhang, Q.; Jia, X.; Xi, K. One-pot synthesis and control of aqueous soluble and organic soluble carbon dots from a designable waterborne polyurethane emulsion. *Nanoscale* **2016**, *8*, 3973-3981.
(6) Zhang, J.; Yu, S. -H. Carbon dots: Large-scale synthesis, sensing and bioimaging. *Mater. Today* **2016**, *19*, 382-393.
(7) Cayuela, A.; Soriano, M. L.; Carillo-Crion, C.; Valcarcel, M. Semiconductor and carbon-based fluorescent nanodots: The need for consistency. *Chem. Commun.* **2016**, *52*, 1311-1326.
(8) Das, R.; Bandyopadhyay, R.; Pramanik, P. Carbon quantum dots from natural resource: A review. *Mater. Today Chem.* **2018**, *8*, 96-109
(9) Zheng, X. T.; Ananthanarayanan, A.; Luo, K. Q.; Chen, P. Glowing graphene quantum dots and carbon dots: Properties, Syntheses, and biological applications. *Small* **2015**, *11*, 1620-1636.
(10) Zhai, X.; Zhang, P.; Liu, C.; Bai, T.; Li, W.; Dai, L.; Liu, W. Highly luminescent carbon nanodots by microwave-assisted pyrolysis. *Chem. Commun.* **2012**, *48*, 7955-795.
(11) Skaltsas, T.; Stergiou, A.; Chronopoulos, D. D.; Zhao, S.; Shinohara, H.; Tagmatarchis, N. All-carbon nanosized hybrid materials: Fluorescent carbon dots conjugated to multiwalled carbon nanotubes. *J. Phys. Chem. C* **2016**, *120*, 8550-8558.
(12) Arcudi, F.; Strauss, V.; Dordevic, L.; Cadranel, A.; Guldi, D. M.; Prato, M. Porphyrin antennas on carbon nanodots: Excited state energy and electron transduction. *Angew. Chem. Int. Ed.* **2017**, *56*, 12097-12101.
(13) Ferrer-Ruiz, A.; Schari, T.; Haines, P.; Rodriguez-Perez, L.; Cadranel, A.; Herranz, M. A.; Guldi, D. M.; Martin, N. Exploring tetrathiafulvalene-carbon nanodot conjugates in charge transfer reactions. *Angew. Chem. Int. Ed.* **2018**, *57*, 1001-1005.
(14) Baker, S. N.; Baker, G. A. Luminescent carbon nanodots: Emerging nanolights. *Angew. Chem. Int. Ed.* **2010**, *49*, 6726-6744.
(15) Strauss, V.; Margraf, J. T.; Dolle, C.; Butz, B.; Nacken, T. J.; Walter, J.; Bauer, W.; Peukert, W.; Spiecker, E.; Clark, T.; Guldi, D. M. Carbon nanodots: Toward a comprehensive understanding of their photoluminescence. *J. Am. Chem. Soc.* **2014**, *136*, 17308-17316.
(16) Strauss, V.; Margraf, J. T.; Clark, T.; Guldi, D. M. A carbon-carbon hybrid – immobilizing carbon nanodots onto carbon nanotubes. *Chem. Sci.* **2015**, *6*, 6878-6885.
(17) Strauss, V.; Margraf, J. T.; Dirian, K.; Syrgiannis, Z.; Prato, M.; Wessendorf, C.; Hirsch, A.; Clark, T.; Guldi, D. M. Carbon nanodots: Supramolecular electron donor-acceptor hybrids featuring perylenediimides. *Angew. Chem. Int. Ed.* **2015**, *54*, 8292-8297.
(18) Cadranel, A.; Strauss, V.; Margraf, J. T.; Winterfeld, K. A.; Vogl, C.; Dordevic, L.; Arcudi, F.; Hoelzel, H.; Jux, N.; Prato, M.; Guldi, D. M. Screening supramolecular interactions between carbon nanodots and porphyrins. *J. Am. Chem. Soc.* **2018**, *140*, 904-907.
(19) Pumera, M.; Sofer, Z.; Ambrosi, A. Layered transition metal dichalcogenides for electrochemical energy generation and storage. *J. Mater. Chem. A* **2014**, *2*, 8981-8987.
(20) Perivoliotis, D. K.; Tagmatarchis, N. Recent advancements in metal-based hybrid electrocatalysts supported on graphene and related 2D materials for the oxygen reduction reaction. *Carbon* **2017**, *118*, 493-510.
(21) Lv, R.; Robinson, J. A.; Schaak, R. E.; Sun, D.; Sun, Y.; Mallouk, T. E.; Terrones, M. Transition metal dichalcogenides and beyond: Synthesis, properties, and applications of single- and few-layer nanosheets. *Acc. Chem. Res.* **2015**, *48*, 56-64.
(22) Jariwala, D.; Sangwan, V. K.; Lauhon, L. J.; Marks, T. J.; Hersam, M. C. Emerging applications for semiconducting two-dimensional transition metal dichalcogenides. *ACS Nano* **2014**, *8*, 1102-1120.
(23) Wang, Q. H.; Kalantar-Zadeh, K.; Kis, A.; Coleman, J. N.; Strano, M. S. Electronics and optoelectronics of two-dimensional transition metal dichalcogenides. *Nat. Nanotechnol.* **2012**, *7*, 699.
(24) Duong, D. L.; Yun, S. J.; Lee, Y. H. van der Waals layered materials: Opportunities and challenges. *ACS Nano* **2017**, *11*, 11803-11830.
(25) Miro, P.; Audiffred, M.; Heine, T. An atlas of two-dimensional materials. *Chem. Soc. Rev.* **2014**, *43*, 6537-6554.
(26) Chhowalla, M.; Shin, H. S.; Eda, G.; Li, L. J.; Loh, K. P.; Zhang, H. The chemistry of two-dimensional layered transition metal dichalcogenide nanosheets. *Nat. Chem.* **2013**, *5*, 263-275.
(27) Grayfer, E. D.; Kozlova, M. N.; Fedorov, V. E. Colloidal 2D nanosheets of MoS_2 and other transition metal dichalcogenides through liquid-phase exfoliation. *Adv. Colloid Interface Sci.* **2017**, *245*, 40-61.
(28) Tao, H.; Zhang, Y.; Gao, Y.; Sun, Z.; Yan, C.; Texter, J. Scalable exfoliation and dispersion of two-dimensional materials – an update. *Phys. Chem. Chem. Phys.* **2017**, *19*, 921-960.
(29) Niu, L.; Coleman, J. N.; Zhang, H.; Shin, H.; Chhowalla, M.; Zheng, Z. Production of two-dimensional nanomaterials via liquid-based direct exfoliation. *Small* **2016**, *12*, 272-293.
(30) Zhang, X.; Lai, Z.; Tan, C.; Zhang, H. Solution-processed two-dimensional MoS2 nanosheets: Preparation, hybridization, and applications. *Angew. Chem. Int. Ed.* **2016**, *55*, 8816-8838.
(31) Fan, X.; Xu, P.; Li, Y. C.; Zhou, D.; Sun, Y.; Nguyen, M. A. T.; Terrones, M.; Mallouk, T. E. Controlled exfoliation of MoS_2 crystals into trilayer nanosheets. *J. Am. Chem. Soc.* **2016**, *138*, 5143-5149.
(32) Pagona, G.; Bittencourt, C.; Arenal, R.; Tagmatarchis, N. Exfoliated semiconducting pure 2H-MoS_2 and 2H-WS_2 assisted by chlorosulfonic acid. *Chem. Commun.* **2015**, *51*, 12950-12953.
(33) Ryder, C. R.; Wood, J. D.; Wells, S. A.; Hersam, M. C. Cehmically tailoring semiconducting two-dimensional transition metal dichalcogenides and black phosphorus. *ACS Nano* **2016**, *10*, 3900-3917.
(34) Bertolazzi, S.; Gobbi, M.; Zhao, Y.; Backes, C.; Samori, P. Molecular chemistry approaches for tuning the properties of two-dimensional transition metal dichalcogenides. *Chem. Soc. Rev.* **2018**, *47*, 6845-6888.
(35) Xin, C.; McDonald. A. R. Functionalization of two-dimensional dichalcogenides. *Adv. Mater.* **2016**, *28*, 5738-5746.
(36) Knirsch, K. C.; Berner, N. C.; Nerl, H. C.; Cucinotta, C. S.; Gholamvand, Z.; McEvoy, N.; Wang, Z.; Abramovic, I.; Vecera, P.; Halik, M.; Sanvito, S.; Duesberg, G. S.; Nicolosi, V.; Hauke, F.; Hirsch, A.; Coleman, J. N.; Backes, C. Basal-plane functionalization of chemically exfoliated molybdenum disulfide by diazonium salts. *ACS Nano* **2015**, *9*, 6018-6030.
(37) Backes, C.; Berner, N. C.; Chen, X.; Lafargue, P.; LaPlace, P.; Freeley, M.; Duesberg, G. S.; Coleman, J. N.; McDonald, A. R. Functionalization of liquid-exfoliated two-dimensional 2H-MoS_2. *Angew. Chem. Int. Ed.* **2015**, *54*, 2638-2642.
(38) McAdams, S. G.; Lewis, E. A.; Brent, J. R.; Haigh, S. J.; Thomas, A. G.; O'Brien, P.; Tuna, F.; Lewis, D. J. Dual functionalization of liquid-exfoliated semiconducting 2H-MoS_2 with lanthanide complexes bearing magnetic and luminescence properties. *Adv. Funct. Mater.* **2017**, *27*, 1703646.
(39) Canton-Vitoria, R.; Sayed-Ahmad-Baraza, Y.; Pelaez-Fernandez, M.; Arenal, R.; Bittencourt, C.; Ewels, C. P.; Tagmatarchis, N. Functionalization of MoS_2 with 1,2-dithiolanes: Toward donor-acceptor nanohybrids for energy conversion. *NPJ 2D Mater. App.* **2017**, *1*, 13.
(40) Canton-Vitoria, R.; Vallan, L.; Urriolabeitia, E.; Benito, A. M.; Maser, W. K.; Tagmatarchis, N. Electronic interactions in illuminated carbón dot/MoS_2 ensembles and electrocatalytic activity towards hydrogen evolution. *Chem. Eur. J.* **2018,** *24*, 10468-10474.
(41) Canton-Vitoria, R.; Stangel, C.; Tagmatarchis, N. Electrostatic association of ammonium-functionalized layered-transition-

metal dichalcogenides with an anionic porphyrin. *ACS Appl. Mater. Interf*aces **2018**, *10*, 23476-23480.
(42) Li, H.; Zhang, Q.; Chong, R. Y. C.; Beng, K. T.; Hang, T. E. T.; Olivier, A.; Baillargeat. D. From bulk to monolayer MoS_2: Evolution of Raman scattering. *Adv. Funct. Mater*. **2012,** *22*, 1385-1390.
(43) Benson, E. E.; Zhang, H.; Schuman, S. A.; Nanayakkara, S. U.; Bronstein, N. D.; Ferrere, S.; Blackburn, J. L.; Miller, E. M. Balancing the hydrogen evolution reaction, surface energietics, and stability of metallic MoS_2 nanosheets via covalent functionalization. *J. Am. Chem. Soc*. **2018**, *140*, 441-450.
(44) Nayak, A. P.; Pandey, T.; Voiry, D.; Liu, J.; Moran, S. T.; Sharma, A.; Tan, C.; Chen, C.-H.; Li, L.-J.; Chhowalla, M.; Lin, J.-F.; Singh, A. K.; Akinwande, D. Pressure-dependent optical and vibrational properties of monolayer molybdenum disulfide. *Nano Lett.* **2015**, *15*, 346-353.
(45) Jimenez Sandoval, S.; Yang, D.; Frindt, R. F.; Irwin, J. C. Raman study and lattice dynamics of single molecular layers of MoS_2. *Phys. Rev. B* **1991**, *44*, 3955-3962.
(46) Chakraborty, B.; Bera, A.; Muthu, D. V. S.; Bhowmick, S.; Waghmare, U. V.; Sood, A. K. Symmetry-dependent phonon renormalization in monolayer MoS_2. *Phys. Rev. B: Condens. Matter*. **2012**, *85*, 161403.
(47) Shi, Y.; Huang, J.-K.; Jin, L.; Hsu, Y.-T.; Yu, S. F.; Li, L.-J.; Yang, H. Y. Selective decoration of Au nanoparticles on monolayer MoS_2 single crystals. *Sci. Rep*. **2013**, *3*, 1839.
(48) Arenal, R.; De Matteis, L.; Custardoy, L.; Mayoral, A.; Tence, M.; Grazu, V.; de la Fuente, J. M.; Marquina, C.; Ibarra, M. R. Spatially-resolved EELS analysis of antibody distribution on biofunctionalzied magnetic nanoparticles. *ACS Nano* **2013**, *7*, 4006-4013.
(49) Arenal, R.; March, K.; Ewels, C. P.; Rocquefelte, X.; Kociak, M.; Loiseau, A.; Stephan, O. Atomic configuration of nitrogen-doped single-walled carbon nanotubes. *Nano Lett.* **2014**, *14*, 5509-5516.
(50) Wibmer, L.; Lages, S.; Unruh, T.; Guldi, D. M. Excitons and trions in one-photon- and two-photon-excited MoS_2: A study in dispersions. *Adv. Mater.* **2018**, *30*, 1706702.
(51) Chowdhury, R. K.; Nandy, S.; Bhattacharya, S.; Karmakar, M.; Bhaktha, B. N. S.; Datta, P. K.; Taraphder, A.; Ray, S. K. Broadband pump-probe study of biexcitons in chemically exfoliated layered WS_2. *Cond. Mater*. **2018**, 1-8.
(52) Jiang, T.; Chen, R.; Zheng, X.; Xu, Z.; Tang, Y. Photo-induced excitonic structure renormalization and broadband absorption in monolayer tungsten disulphide. *Optics Expr*. **2018**, *26*, 859-869.
(53) Homan, S. B.; Sangwan, V. K.; Balla, I.; Bergeron, H.; Weiss, E. A.; Hersam, M. C. Ultrafast exciton dissociation and long-lived charge separation in a photovoltaic pentacence-MoS_2 van der Waals heterojunction. *Nano Lett.* **2017**, *17*, 164-169.
(54) Kafle, T. R.; Kattel, S.; Lane, S. D.; Wang, T.; Zhao, H.; Chan, W.-L. Charge-transfer exciton and spin flipping at organic-transition-metal dichalcogenide interfaces. *ACS Nano* **2017**, *11*, 10184-10192.
(55) Nguyen, E. P.; Carey, B. J.; Harrison, C. J.; Atkin, P.; Berean, K. J.; Gaspera, E. D.; Ou, J. Z.; Kaner, R. B.; Kalantar-zadeh, K.; Daeneke, T. Excitation dependent bidirectional electron transfer in phthalocyanine MoS_2 nanosheets. *Nanoscale* **2016**, *8*, 16276-16283.
(56) Choi, J.; Zhang, H.; Choi, J. H. Modulating optoelectronic properties of two-dimensional transition metal dichalcogenide semiconductors by photoinduced charge transfer. *ACS Nano* **2016**, *10*, 1671-1680.

ToC